SAND2017-8430C

Annualized Thermal Performance of Intermediate-Scale Falling Particle Receivers

Brantley Mills[(a)] and Clifford K. Ho

Sandia National Laboratories, P.O. Box 5800, MS-0836, Albuquerque, NM 87185-0836, USA

[(a)]Corresponding author: bramill@sandia.gov

Abstract. A computational fluid dynamics model of a 50 MWe falling particle receiver has been developed to evaluate the ability of the receiver concept to scale to intermediate sized systems while maintaining high thermal efficiencies. A compatible heliostat field for the receiver was generated using NREL's SolarPILOT, and this field was used to calculate the irradiance on the receiver at seventeen different dates and times throughout the year. The thermal efficiency of the receiver was evaluated at these seventeen different samples using the CFD model and found to vary from 83.0 – 86.6%. An annualized thermal efficiency was calculated from the samples to be 85.7%. A table was also generated that summarized this study along with other similar CFD studies on falling particle receivers over a wide ranges of scales.

INTRODUCTION

A north-facing 50 MWe falling particle receiver (FPR) is proposed and evaluated using a computational fluid dynamics (CFD) model to better understand the thermal performance of intermediate-scale FPRs. The use of high-temperature FPRs for future concentrating solar power applications is being studied primarily for their potential to operate at high temperatures with high thermal efficiencies using a low cost heat transfer medium [1,2,3]. Traditional designs for receivers typically circulate a working fluid through irradiated pipes but are often limited by thermal and mechanical limitations of the structural materials. However, in falling particle receiver designs, commercially available and inexpensive ceramic particles are directly heated by the concentrated solar radiation as they fall through a receiver cavity avoiding many constraints imposed by traditional systems.

The conventional strategy to heat the particles in a FPR has been to release them in a planar curtain from the top of a receiver cavity and let them fall through the concentrated sunlight. Experiments on smaller FPRs have demonstrated the ability to achieve very high particle outlet temperatures (>700°C) [4] using this strategy supporting use with high efficiency supercricial-CO_2 cycles. However, experiments for significantly larger systems (≥ 10 MWe) have not yet been performed. Of particular interest is the ability of these receivers to scale while sustaining high thermal efficiencies over the calendar year as has been explored in some other works on FPR designs [5]. Other studies have investigated very large FPRs (≥ 100 MWe) using CFD models, but suitable receiver designs with high thermal efficiencies were not immediately found [6]. This work samples the thermal efficiency of the candidate 50 MWe receiver at different dates and times throughout the year to support the scalability of intermediate sized FPRs.

This remainder of this paper is organized as follows. First, a description of the FPR CFD model is provided along with the development of a compatible heliostat field. Next, this model is utilized to evaluate the thermal performance and heat losses from the design at various dates and times throughout the year. Then, the annualized thermal efficiency is calculated, and the results of this study are summarized with similar studies of FPRs at different scales found in the literature. Finally, the conclusions of this study are summarized.

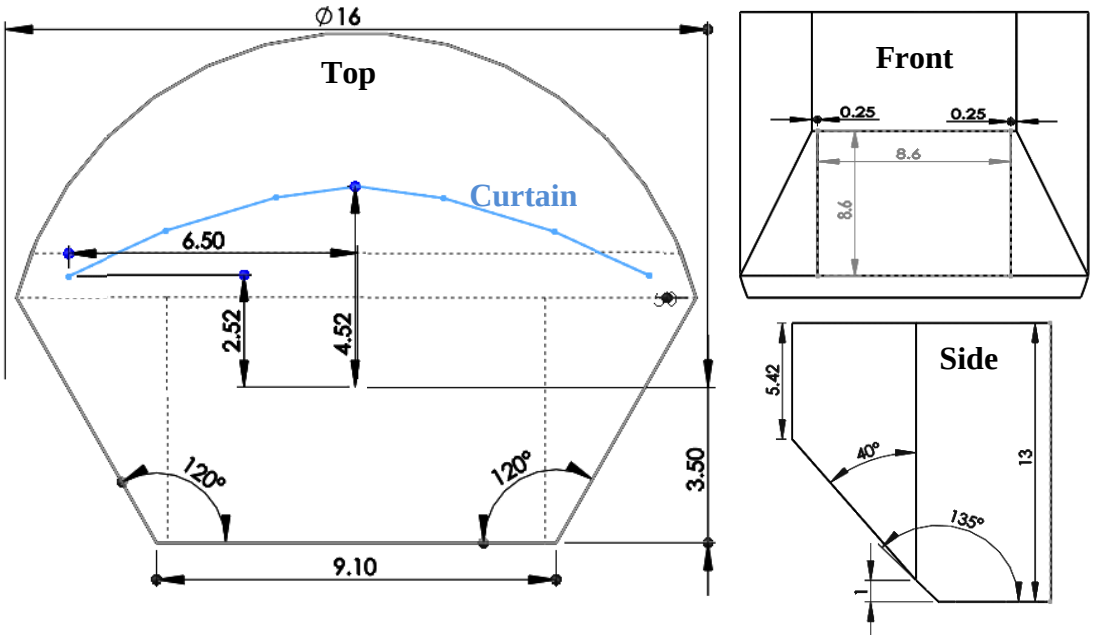

FIGURE 1. Drawing of the proposed falling particle receiver viewed from the top (left image) from the side (bottom right image) and the front (top right image). Units in meters

COMPUTATIONAL MODEL DESCRIPTION

This section describes the modeling strategy used to simulate the thermal performance of the candidate 50 MWe FPR. This strategy is similar to other modeling efforts for FPRs using ANSYS Fluent® found in the literature [7,8]. The dimensions of the proposed receiver are provided in addition to a description of the CFD model. Irradiative boundary conditions to the CFD model are determined from an optimized heliostat field generated using SolarPILOT developed by the National Renewable Energy Laboratory [9].

Falling Particle Receiver CFD Model

A dimensioned drawing of the receiver cavity is provided in FIGURE 1. A square aperture of 8.6 m x 8.6 m with a nod angle of 40° was chosen to minimize the total number of heliostats and simultaneously reduce convective losses from the receiver based on the conclusions reached in Reference 6. A curved receiver cavity was selected to support curvature in the falling particle curtain.

The air volume inside the receiver cavity was modeled and comprised of 420,464 hexahedral cells. Air entered or exited the receiver through the aperture and circulated throughout the receiver cavity from entrainment with the falling particles or from buoyancy-driven flow resulting from temperature gradients within the air. Turbulent flow was modeled using the realizable k-ε turbulence model and Fluent's scalable wall functions, which have been applied in other validated FPR models albeit at lower temperatures and fluxes [7]. The receiver walls were modeled entirely as alumina silica ceramic fiberboard (0.0508 m thick). To more accurately characterize convective losses from the receiver, an external air domain just outside of the receiver surrounding the aperture was also included in the model. Including an external air domain was critical to capturing heated air leaving the aperture that is recirculated back into the receiver [6]. This external air domain was comprised of 92,852 hexahedral cells, and fixed pressure boundary conditions were applied to the exterior boundaries with an ambient temperature of 300 K.

Particles were released from 600 injection sites defined near the top of the receiver cavity and tracked through the domain before exiting out of the hopper. Specified particles for the receiver were CARBO HSP 20/40 (82% Al_2O_3,

5% SiO_2, 3.5% TiO_2) with ~7% iron oxide with particle diameters of 700 μm, and their material properties were taken from Reference 7. Note that particles exited the domain when they came in contact with any surface of the hopper. That is, particle bouncing within the hopper was not modeled as it would add significant computational effort without confidence that the particle motion could be accurately captured. Each particle's motion was coupled with the air through drag forces acting on the particles. Particle to particle interaction was not included under the assumption that the volume fraction of particles in the air volume was sufficiently small. This assumption was valid for volume fractions less than 10% [10]. For this study, particle inlet temperatures were set to 575°C (848 K), and the mass flow rate was varied such that the average particle outlet temperature was between 750-775°C for a given date and time. A curved particle release curtain was applied in this receiver with a total particle curtain length of 13.95 m. The curved curtain was comprised of six linear segments, and the profile is depicted in FIGURE 1.

A non-grey discrete-ordinates radiation model was used to simulate radiation heat transfer inside the domain. Both angular dimensions were discretized into eleven divisions per octant. The wavelength spectrum was divided into two spectral bands: 0.1 – 4.5 μm and 4.5 – 100 μm to more accurately represent the spectral properties of the alumina silica ceramic fiberboard receiver walls. All incident solar radiation was defined to enter the domain entirely in the smaller wavelength band (0.1 – 4.5 μm). The second, higher wavelength band was used to define the emission of thermal radiation.

Incident solar radiation to the domain was applied as a boundary condition on the aperture surface. The entire aperture was defined to emit the concentrated solar radiation with a profile determined from SolarPILOT for a given date and time and an optimized heliostat field layout (described below). The incident beam shape and direction emitted from a cell face on the aperture was determined using the method described by Khalsa and Ho [11] for the heliostat field defined in SolarPILOT. Conduction through the walls of the receiver was also included in the model in addition to convection on the exterior walls to the surrounding environment. A heat transfer coefficient of 5 W/m^2K was applied on the exterior of the receiver with a reference temperature of 300 K. This analysis did not account for external winds and assumed natural convection on the exterior walls.

Heliostat Field Layout

A north facing receiver was chosen for this analysis, and a compatible heliostat field layout was generated using the optimization capability found in SolarPILOT. Assumptions for much of the solar field including the size and characteristics for the heliostats were selected from a Black & Veatch report for a proposed 10 MWe receiver [12]. These heliostats were single pedestal designs with a reflective area of 96 m^2 and a total optical reflectance of 90%. A limb-darkened sun shape model and DELSOL3's atmospheric attenuation model was applied assuming a clear day.

For a 50 MWe north-facing plant, it was assumed that 135 MW_{th} peak thermal power would be delivered to the aperture on the equinox at solar noon. For a FPR with a thermal efficiency of ~90%, this would deliver a peak ~121.5 MW_{th} to the power cycle. Assuming that this plant would be coupled with a supercritical-CO_2 cycle with an efficiency of ~50%, then a heliostat field of this size provided a peak solar multiple of ~1.2 for thermal storage. Using this as a design point for the heliostat field, the optimum year-round field layout for the receiver was determined for Albuquerque, NM, USA. The heliostat layout from this optimization is depicted in FIGURE 2. A total of 2,529 heliostats were defined with a total reflective area of 61,466 m^2. The solar tower had an optical height of 145.0 m.

SolarPILOT was used to simulate the radiative boundary conditions on the aperture for seventeen distinct dates and times throughout the year. These samples primarily consisted of different times of the day on the equinox or solstice, but a few samples were also included in between these dates. The precise dates and times are provided later. Including further samples was deemed too computationally expensive for a model of this size. The position of the sun for each sample was described in terms its declination δ (in radians) and hour angle ω (in radians) as approximated below with the following equations [13]:

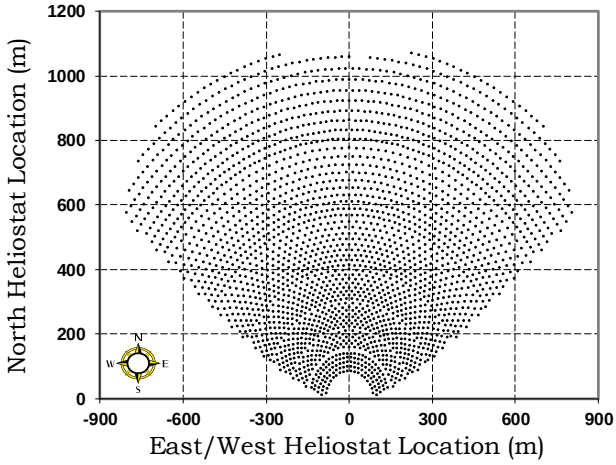

FIGURE 2. Optimized heliostat field layout from SolarPILOT

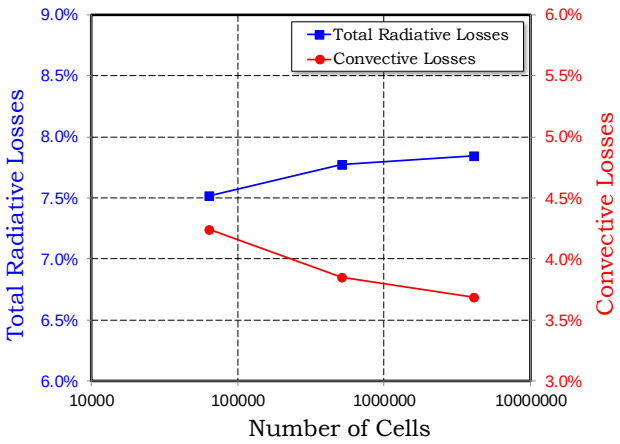

FIGURE 3. Total radiative and convective losses as the mesh is uniformly refined for each mesh

$$\delta = \frac{23.45\pi}{180}\sin\left(360\cdot\left(\frac{284+n}{365}\right)\right) \tag{1}$$

and

$$\omega = \frac{15\pi}{180}t \tag{2}$$

where n is the day of the year from 1 to 265, and t is the time from solar soon from -12 to +12. The maximum number of daylight hours for a given day t_{max} is approximated by [13]:

$$t_{\max} = \frac{24}{\pi}\cos^{-1}\left(-\tan(\delta_{lat})\tan(\delta)\right) \tag{3}$$

where δ_{lat} = 34.5° is the latitude for Albuquerque, NM.

Mesh Convergence Study

In order to have more confidence that the mesh resolution was sufficient to provide a converged solution, a mesh convergence study was performed. A similar convergence study was performed in Mills and Ho [14] for a significantly smaller scale receiver design showing that the thermal losses from convection and radiation were converging with decreasing mesh size. Differences in the application of the solar radiation boundary condition in this model compared with this preceding study limited the meshes explored to uniformly refined meshes. Unfortunately, this added significant computational expense as the mesh was refined. Each mesh explored in this study consisted of either 64,177, 513,416, or 4,107,328 cells. The responses of interest in this investigation included the total radiative and convective losses from the model with increasing cell counts for the vernal equinox at solar noon.

The total radiative and convective losses in the model are plotted in FIGURE 3 for each of the three meshes. As observed in the figure, both loss mechanisms were showing convergence as the mesh resolution was increased. Given the large computational expense for the most refined mesh and the small differences in solution for both loss mechanisms between the two most refined meshes (< 0.2%-points), it was deemed that the second most refined mesh was sufficient to evaluate the thermal performance (*i.e.* 513,416 cells). That is, any error introduced from the mesh resolution was considered within other model-form errors and could be neglected.

MODELING RESULTS

The thermal efficiency of the receiver is defined as the fraction of incident thermal radiative power that is removed by the particles as they exit the receiver. That is:

$$\eta_{th} = \frac{Q_{abs}}{Q_{in}} = \frac{\dot{m}(h_{out} - h_{in})}{Q_{in}} = \frac{\int_{T_{in}}^{T_{out}} c_P(T)dT}{Q_{in}} \tag{4}$$

where Q_{abs} is the absorbed thermal power in the particles, Q_{in} is the incident thermal radiative power, $\dot{m}$ is the total particle mass flow rate, h is the enthalpy of the particles, and $c_P(T)$ is the specific heat of the particles (J/kg·K) as a function of temperature T defined as:

$$c_P(T) = 365 \cdot T^{0.18} \tag{5}$$

where T is the mean particle temperature (ºC) for 50ºC $\leq T \leq$ 1100ºC. The thermal efficiency is effectively the fraction of incident radiative power that is removed from the receiver by the particles.

Preliminary simulations were performed at a single design point (equinox at solar noon) to optimize the receiver height and the particle curtain location within the receiver. Receiver heights were varied from 11 – 14 m (a nominal value of 13 m was selected), and seven different curtain configurations were explored. The details of this design process were excluded for brevity. The thermal efficiency of the receiver and the average particle outlet temperature during the equinox, summer solstice, and winter solstice at different times of the day are all plotted in FIGURE 4. As observed in the figure, the thermal performance of the receiver was relatively constant throughout the calendar year with the peak thermal performance observed at solar noon corresponding to higher thermal power delivered to the particles. The thermal efficiency of the receiver varied between 83.0% – 86.6% for all of the seventeen samples. To achieve the desired average particle outlet temperature (750 – 775°C), the particle mass flow rate varied between 25.7 – 36.6 kg/m·s.

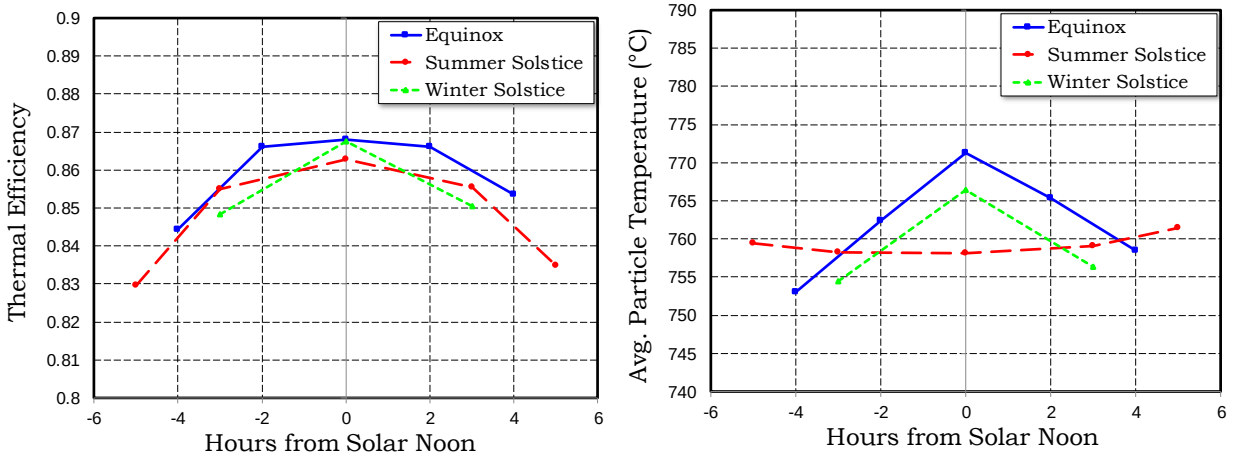

FIGURE 4. Average particle outlet temperature and thermal efficiency of the receiver at various dates and times throughout the year

The thermal losses from each loss mechanism in the model were evaluated at solar noon for the equinox, summer solstice, and winter solstice at solar noon and plotted in FIGURE 5. Nominal particle sizes of 700 µm were modeled in this study, but smaller particle sizes of 500 µm were also explored for their improved radiative performance. Also included in the figure are the losses for particle sizes of 500 µm, and particle absorptivities α of 0.5 and 0.9 (compared to the nominal value of 0.8) at the equinox as well. Ultimately, very little variation in the losses was observed for the different seasons, but smaller particle sizes showed lower radiative losses in the smaller wavelength band offset by

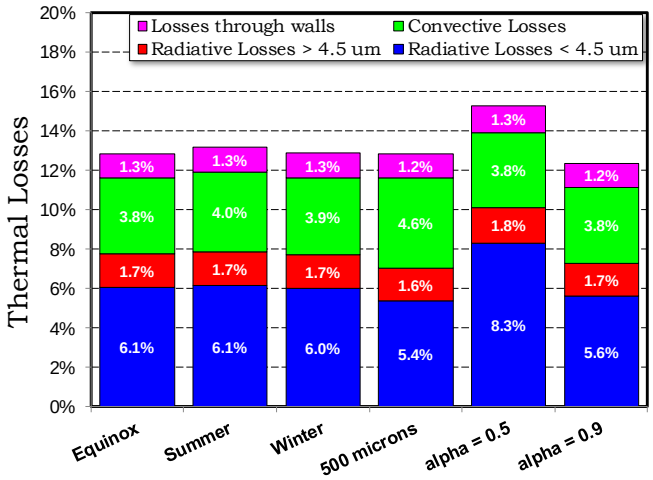

FIGURE 5. Thermal losses from different loss mechanisms in the model

increased convective losses. For particle absorptivities as low as 0.5, radiative losses in the smaller wavelength band only increased by approximately 2.2%-points.

ANNUALIZED PERFORMANCE

Using the discrete samples described above, an estimated annualized thermal efficiency was calculated for the receiver design to evaluate its thermal performance throughout the year as opposed to only a single design point. The sun's position throughout the year, defined by its declination δ and hour angle ω (Eqs. 1 and 2, respectively), was divided into six minute increments. Each increment was then binned with the closest corresponding sun position of the seventeen samples. Then, each bin was assigned with that sample's thermal efficiency, and the bins were appropriately averaged to calculate an annualized thermal efficiency. Visually this weighting is shown in FIGURE 6. The dashed lines on either side of the figure defined the amount of available sunlight hours in the day as calculated by Eq. 3. Note that the declination of the sun does not vary linearly throughout the year; therefore, the samples at the solstices ($\delta \approx 0.41\ or\ -0.41$) were weighted more heavily than they appear in the figure. In addition, given that the receiver thermal efficiency decreased as the time moved further from solar noon, this method had a tendency to overestimate the thermal efficiency of the receiver near the beginning and end of the day. However, this effect was less significant since the total thermal power incident on the receiver at those times was small. The annualized thermal efficiency for this receiver was calculated to be 85.7% supporting the scalability of FPRs to intermediate-scales.

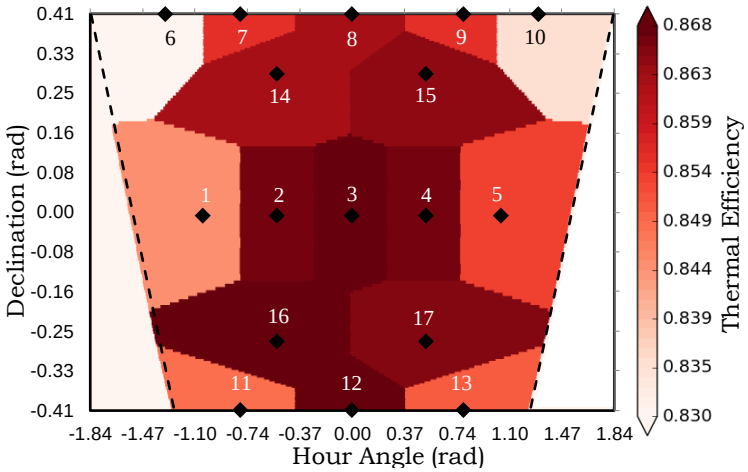

1. Equinox: -4 hrs.
2. Equinox: -2 hrs.
3. Equinox: solar noon
4. Equinox: +2 hrs.
5. Equinox: +4 hrs.
6. Summer solstice: -5 hrs.
7. Summer solstice: -3 hrs.
8. Summer solstice: solar noon
9. Summer solstice: +3 hrs.
10. Summer solstice: +5 hrs.
11. Winter solstice: -3 hrs.
12. Winter solstice: solar noon
13. Winter solstice: +3 hrs.
14. May 6: -2 hrs.
15. May 6: +2 hrs.
16. November 1: -2 hrs.
17. November 1: +2 hrs.

FIGURE 6. Depiction of the seventeen weighted dates and times for an annualized thermal efficiency of 85.7%

The results of this study added to a growing list of other numerical studies on FPRs at many different scales that evaluated the thermal efficiency of these designs. To summarize the multitude of other studies and illustrate how this receiver study fits in with the larger picture, a summary table of known FPR studies in the literature has been created and provided in TABLE 1. For more information on each of these individual studies, references have been provided.

TABLE 1. Summary table of falling particle receiver studies at different scales

Falling Particle Receiver Models at Various Scales	1-2.5 MW_{th}	10 MWe	50 MWe	100 MWe
	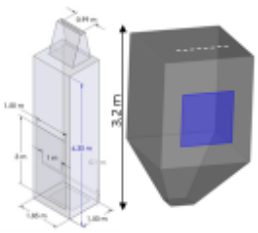	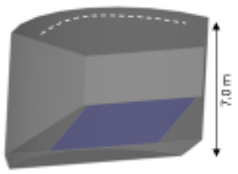	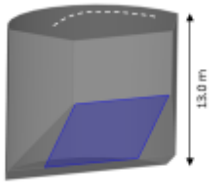	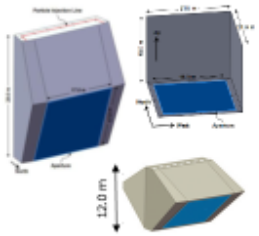
Reported Efficiencies	~35% - 53% [7], 44.7% - 52.9% [15,16], 86.3% - 89.5% [14]	70.1% - 87.6% Annual value: 85.0%	83.0% - 86.8% Annual value: 85.7%	North-Facing: 72.3% [8], 69.7% - 86.8% [6]; Face Down: 78.9% [8]
Model Description	A coupled Lagrangian-Eulerian CFD model is used to predict the behavior of the particles as they fall through the air in the receiver cavity. Incident radiation from the solar field is included via a non-grey discrete ordinates radiation model. Losses from the receiver include exterior convection, radiative losses from reflections or thermal emissions, and convective losses from the particles to the air.			
Notable Features	• Aperture: 3.0 x 1.0 m; 1.0 x 1.0 m • Nod angle: 0° • Validated w/ low temp. data [7] • More prototypical design [14] • Investigated novel particle curtain release patterns [14-16] • D_{part} = 280 – 697 µm • Design tested at NSTTF [5]	• Aperture: 5.6 x 5.6 m • Nod angle: 50° • Curved particle curtain, 7.89 m • NREL's SolarPILOT used to generate compatible solar field • D_{part} = 697 µm • Heliostat #: 640 • Eff. evaluated over calendar year	• Aperture: 8.6 x 8.6 m • Nod angle: 40° • Curved particle curtain, 13.95 m • NREL's SolarPILOT used to generate compatible solar field • D_{part} = 500 – 697 µm • Heliostat #: 2,529 • Eff. evaluated over calendar year	• Investigated North-Facing (NF) and Face Down (FD) designs [8] • Aperture: NF: 10.6 x 10.6 m - 17.0 x 17.0 m; FD: 18.0 x 18.0 m • NF Nod angle: 20° - 50° • Investigated particle recirculation • D_{part} = 697 µm • Heliostat #: 3,242 – 7,183
Sources	[5], [7], [14], [15], [16]	[17]	[Present study]	[6], [8]

CONCLUSIONS

A candidate 50 MWe falling particle receiver has been proposed in this work to evaluate the thermal efficiency of falling particle receivers as they scale to intermediate sizes. A computational fluid dynamics model of the receiver design was developed in ANSYS Fluent utilizing a discrete ordinates radiation model to model incident solar radiation. NREL's SolarPILOT was used to create a suitable heliostat field and define the radiative boundary conditions to the receiver. The model was used to calculate the thermal efficiency of the receiver defined as the radiative power transferred to the particles.

The thermal performance was evaluated at seventeen discrete dates and times throughout the year, and the thermal efficiency varied from 83.0 – 86.8% for particle mass flow rates of varying from 25.7 – 36.6 kg/m·s and average particle outlet temperatures 750 – 775°C. An annualized thermal efficiency was also estimated for this receiver design from the seventeen samples to be 85.7%. This annualized thermal efficiency, with minimum optimization performed on the design, supports the ability of falling particle receivers to scale to intermediate sizes.

ACKNOWLEDGMENTS

Sandia National Laboratories is a multi-mission laboratory managed and operated by National Technology and Engineering Solutions of Sandia, LLC., a wholly owned subsidiary of Honeywell International, Inc., for the U.S. Department of Energy's National Nuclear Security Administration under contract DE-NA0003525.

REFERENCES

1. C. Ho, J. Christian, D. Gill, A. Moya, S. Jeter, S. Abdel-Khalik, D. Sadowski, N. Siegel, H. Al-Ansary, L. Amsbeck, B. Gobereit and R. Buck, *Technology advancements for next generation falling particle receivers*, Proceedings of the SolarPACES 2013 International Conference **49**, 398-407 (2014).
2. T. D. Tan and Y. T. Chen, Review of study on solid particle solar receivers, Renew Sust Energ Rev 14 (1), 265-276 (2010).
3. J. Christian and C. K. Ho, *Design Requirements, Challenges, and Solutions for High-Temperature Falling Particle Receivers*, in *SolarPACES 2015 Conference*, Cape Town, South Africa, October 13-16, 2016.
4. Ho, C.K., J.M. Christian, J. Yellowhair, K. Armijo, and S. Jeter, 2016, *Performance Evaluation of a High-Temperature Falling Particle Receiver*, in *ASME P&E Conference*, Charlotte, NC, June 26-30, 2016.
5. Röger, M., Amsbeck, L., Gobereit, B., Buck, R., "Face-Down Solid Particle Receiver using Recirculation," *Journal of Solar Engineering*, Vol. 133 (2011)
6. Christian, J., and Ho, C., "Alternative designs of a high efficiency, north-facing, solid particle receiver," *Energy Procedia*, **49**, 314 (2014)
7. N. P. Siegel, C. K. Ho, S. S. Khalsa and G. J. Kolb, Development and Evaluation of a Prototype Solid Particle Receiver: On-Sun Testing and Model Validation, J Sol Energ-T Asme 132 (2) (2010).
8. Khalsa, S. S., et al. "CFD Simulation and performance Analysis of Alternative Designs for High-Temperature Solid Particle Receivers," in *ASME Energy Sustainability & Fuel Cell Conference*, Washington DC, August 7-10, 2011.
9. Integrated Layout and Optimization Tool for Solar Power Towers, Concentrating Solar Power, National Renewable Energy Laboratory Website, https://www.nrel.gov/csp/solarpilot.html, Accessed May 2017
10. N. Siegel, G. Kolb, K. Kim, V. Rangaswamy and S. Moujaes, *Solid particle receiver flow characterization studies*, Proceedings of the Energy Sustainability Conference 2007, 877-883 (2007).
11. Khalsa, S. S., and Ho, C. K., "Radiation Boundary Conditions for Computational Fluid Dynamics Models of High-Temperature Cavity Receivers.," Journal of Solar Energy Engineering. 2011
12. Falling Particles: Concept Definition & Capital Cost Estimate, Report Prepared by Black & Veatch, June 30, 2016
13. Duffie, J. A. and Beckman, W. A., Solar Engineering of Thermal Processes, 4th Edition, John Wiley & Sons, 2013
14. Mills, B. H., Ho, C. K., "Numerical Evaluation of Novel Particle Release Patterns in High-temperature Falling Particle Receivers," in *ASME P&E Conference*, Charlotte, NC, June 26-30, 2017
15. C. K. Ho, B. Mills and J. M. Christian, Volumetric Particle Receivers for Increased Light Trapping and Heating, in ASME Power & Energy Conference, Charlotte, NC, June 26-30, 2016.
16. B. Mills, C. K. Ho, J. Christian, G. Peacock, *Novel Particle Release Patterns for Increased Receiver Thermal Efficiency*, in *SolarPACES 2016 Conference*, Abu Dahbi, UAE, June 26-30, 2016.
17. Mills, B. H. and Ho, C. K. "Proposed 10 MWe North-Facing Falling Particle Receiver Design," Sandia National Laboratories Memorandum, disseminated January 10, 2017